VI. Conclusion

We have provided a simple model for magnetic torque and force on soft-magnetic bodies with axial symmetry. The model only requires the knowledge of body geometry and the saturation magnetization of the material. The model handles low and very high applied field intensities well, agreeing with existing models for those regions. In addition and most importantly, it captures the often neglected region between linear and completely saturated behavior. Although constructed from disparate magnetic models, each with its own simplifying assumptions, our model is provably continuous, and the resulting torque and force equations are also continuous. We find that magnetic force can always be increased by increasing the directional derivatives in the applied field. However, there is an upper bound on the magnetic torque that can be generated, due to the shape and magnetic saturation. We provide a formula to compute the optimal applied-field direction to maximize torque for each applied-field magnitude. The simplicity of the presented model will facilitate real-time wireless control, as well as dynamic simulations, without the need for finite-element modeling.

Acknowledgment

The authors would like to thank Z. Nagy and K. Vollmers for their input.

References

[1] J. J. Abbott, Z. Nagy, F. Beyeler, and B. J. Nelson, "Robotics in the small, Part I: Microrobotics," *IEEE Robot. Autom. Mag.*, vol. 14, no. 2, pp. 92–103, Jun. 2007.

[2] K. B. Yesin, K. Vollmers, and B. J. Nelson, "Modeling and control of untethered biomicrorobots in a fluidic environment using electromagnetic fields," *Int. J. Robot. Res.*, vol. 25, no. 5/6, pp. 527–536, 2006.

[3] S. Martel, J.-B. Mathieu, O. Felfoul, A. Chanu, E. Aboussouan, S. Tamaz, and P. Pouponneau, "Automatic navigation of an untethered device in the artery of a living animal using a conventional clinical magnetic resonance imaging system," *Appl. Phys. Lett.*, vol. 90, no. 11, pp. 114105-1–114105-3, 2007.

[4] O. Ergeneman, G. Dogangil, M. P. Kummer, J. J. Abbott, M. K. Nazeeruddin, and B. J. Nelson, "A magnetically controlled wireless optical oxygen sensor for intraocular measurements," *IEEE Sensors J.*, to be published.

[5] K. Ishiyama, K. I. Arai, M. Sendoh, and A. Yamazaki, "Spiral-type micromachine for medical applications," *J. Micromechatron.*, vol. 2, no. 1, pp. 77–86, 2003.

[6] M. Gauthier and E. Piat, "An electromagnetic micromanipulation systems for single-cell manipulation," *J. Micromechatron.*, vol. 2, no. 2, pp. 87–119, 2004.

[7] M. B. Khamesee, N. Kato, Y. Nomura, and T. Nakamura, "Design and control of a microrobotic system using magnetic levitation," *IEEE/ASME Trans. Mechatron.*, vol. 7, no. 1, pp. 1–14, Mar. 2002.

[8] G. T. Gillies, R. C. Ritter, W. C. Broaddus, M. S. Grady, M. A. Howard, III, and R. G. McNeil, "Magnetic manipulation instrumentation for medical physics research," *Rev. Sci. Instrum.*, vol. 65, no. 3, pp. 533–562, 1994.

[9] D. C. Meeker, E. H. Maslen, R. C. Ritter, and F. M. Creighton, "Optimal realization of arbitrary forces in a magnetic stereotaxis system," *IEEE Trans. Magn.*, vol. 32, no. 2, pp. 320–328, Mar. 1996.

[10] S. O. Kasap, *Principles of Electronic Materials and Devices*, 2nd ed. New York: McGraw-Hill, 2002.

[11] D. Jiles, *Introduction to Magnetism and Magnetic Materials*. London, U.K.: Chapman and Hall, 1991.

[12] R. C. O'Handley, *Modern Magnetic Materials: Principles and Applications*. New York: Wiley, 2000.

[13] F. Amblard, B. Yurke, A. Pargellis, and S. Leibler, "A magnetic manipulator for studying local rheology and micromechanical properties of biological systems," *Rev. Sci. Instruments*, vol. 67, no. 3, pp. 818–827, 1996.

[14] R. M. Bozorth, *Ferromagnetism*. Princeton, NJ: Van Nostrand, 1951.

[15] B. D. Cullity, *Introduction to Magnetic Materials*. Reading, MA: Addison-Wesley, 1972.

[16] J. W. Judy, "Batch-fabricated ferromagnetic microactuators with silicon flextures" Ph.D. dissertation, Dept. Elect. Eng. Comput. Sci., Univ. California, Berkeley, 1996.

[17] M. Beleggia, M. De Graef, and Y. T. Millev, "The equivalent ellipsoid of a magnetized body," *J. Phys. D: Appl. Phys.*, vol. 39, pp. 891–899, 2006.

[18] J. A. Osborn, "Demagnetizing factors of the general ellipsoid," *Phys. Rev.*, vol. 67, no. 11/12, pp. 351–357, 1945.

[19] F. Bergmüller, C. Bärlocher, B. Geyer, M. Grieder, F. Heller, and P. Zweifel, "A torque magnetometer for measurements of the high-field anisotropy of rocks and crystals," *Meas. Sci. Technol.*, vol. 5, pp. 1466–1470, 1994.

[20] M. P. Kummer, J. J. Abbott, K. Vollmers, and B. J. Nelson, "Measuring the magnetic and hydrodynamic properties of assembled-MEMS microrobots," in *Proc. IEEE Int. Conf. Robot. Autom.*, 2007, pp. 1122–1127.

Convex Optimization Strategies for Coordinating Large-Scale Robot Formations

Jason C. Derenick and John R. Spletzer

***Abstract*—This paper investigates convex optimization strategies for coordinating a large-scale team of fully actuated mobile robots. Our primary motivation is both algorithm scalability as well as real-time performance. To accomplish this, we employ a formal definition from shape analysis for formation representation and repose the motion planning problem to one of changing (or maintaining) the shape of the formation. We then show that optimal solutions, minimizing either the total distance or minimax distance the nodes must travel, can be achieved through second-order cone programming techniques. We further prove a theoretical complexity for the shape problem of $O(m^{1.5})$ as well as $O(m)$ complexity in practice, where m denotes the number of robots in the shape configuration. Solutions for large-scale teams (1000's of robots) can be calculated in real time on a standard desktop PC. Extensions integrating both workspace and vehicle motion constraints are also presented with similar complexity bounds. We expect these results can be generalized for additional motion planning tasks, and will prove useful for improving the performance and extending the mission lives of large-scale robot formations as well as mobile ad hoc networks.**

***Index Terms*—Barrier method, convex optimization, mobile ad hoc networks, optimal shape formation, second-order cone programming (SOCP), shape change.**

I. Introduction

The robotics community has seen a tremendous increase in multiagent systems research in recent years. This has been driven in part by the maturation of the underlying technology: advances in embedded computing, sensor and actuator technology, and (perhaps most significantly) pervasive wireless communication. However, the primary motivation is the diverse range of applications envisaged for large-scale robot teams, defined herein as formations ranging from tens to

Manuscript received October 11, 2006; revised April 16, 2007. This paper was recommended for publication by Associate Editor B. J. Yi and Editor L. Parker upon evaluation of the reviewers' comments. This paper was presented in part at the IEEE International Conference on Robotics and Automation (ICRA 2005), Barcelona, Spain, April 2005, the 7th International Workshop on the Algorithmic Foundations of Robotics (WAFR 2006), New York, July 2006, and at the 7th International Conference on Cooperative Control and Optimization (CCO 2007), Gainesville, FL, February 2007.

The authors are with the Department of Computer Science and Engineering, Lehigh University, Bethlehem, PA 18015 USA (e-mail: derenick@lehigh.edu; josa@lehigh.edu).

Digital Object Identifier 10.1109/TRO.2007.909833

thousands of robots. These include support of first responders in search and rescue operations, autonomous surveillance and monitoring in support of military and homeland security operations, and environmental monitoring. Unfortunately, the effective coordination of a large-scale robot team is a nontrivial problem—one that will need to be solved in order for such systems to find practical use.

In this paper, we investigate an optimization approach to the coordination task. This is motivated by the realization that the operation of such a team is inherently a constrained resource allocation problem. A (potentially large) number of nodes are required to perform some task (e.g., area surveillance), perhaps with performance objectives (e.g., maximize coverage), while subjected to resources that are restricted by things such as communication and sensor ranges, motion constraints, etc.

While the optimization construct has many advantages, its potential for use in multiagent systems has never been fully realized due to scalability concerns. Complete solutions to problems of interest typically scale in super-linear time with the number of robots and/or the size of the environment. In this paper, we focus on a convex formulation to the problem. By leveraging recent advances in convex optimization theory, we are able to develop motion planning strategies for coordinating a robot team that scale linearly in both the size of the team and/or the environment in practice. The result is a fairly rich framework for coordinating a large-scale team of fully actuated robots in real time.

II. Related Work

Formations of robot teams have been extensively studied in literature, and a complete survey is outside of the scope of this paper. Instead, we focus on those where applications to large-scale robot teams and *shape*—defined differently under different contexts—was of significant relevance to the research. Das *et al*. described a vision-based formation control framework [8]. This focused on achieving and maintaining a given formation shape using a leader-follower framework. Control of formations using Jacobi shape coordinates was addressed by Zhang *et al*. [29]. The approach was applied to a formation of a small number of robots, which were modeled as point masses. Abstraction-based control was used by Belta and Kumar as a mechanism to coordinate a large number of fully actuated mobile robots moving in formation [3]. In this paper, the configuration space of the robots $\mathcal{Q}$ was mapped to a lower dimensional manifold $\mathcal{A}$ to reduce the complexity of the control problem. The concept of *shape* was used in reference to the area spanned by the robots.

In *cooperative control problems*, vehicles move in a coordinated fashion to achieve some common goal and/or seek to maintain some geometrical relationships among themselves. Often motion is dictated by gradient approximations from sensor measurements or an artificial potential field. Solutions defined with interrobot distance relationships were explored by Bachmayer and Leonard [1], where methods to measure and project gradient information were discussed. The applications for these methods are in, for example, data acquisition in large areas such as oceans where the most advantageous arrangement of sensors may not be to distribute them evenly, but to have them adapt to concentrate more sensors in areas where the measured variable has steeper gradients.

There has also been significant interest in applying optimization-based techniques to coordinate robot teams and deploy sensor networks. Contributions in this area include the work by Cortes *et al*. [7]. Here the focus is on autonomous vehicles performing distributed sensing tasks. Recently, Feddema *et al*. applied decentralized optimization-based control to solve a variety of multirobot problems [15]. Optimal motion planning was considered by Belta and Kumar [4]. In this paper, authors generate a family of optimal smooth trajectories for a set of fully actuated mobile robots. The case for which robots have independent goals but share the same space was studied in [21].

In contrast to these efforts, the primary contribution of our research is the application of convex optimization techniques to the coordination task. Using these in conjunction with a formal definition for formation shape, we have developed a framework for coordinating large-scale robot teams that scales in $O(m)$ time in practice, and can calculate optimal formation shape changes in real time for teams with thousands of nodes. With this complexity result, we expect our research will also have applications to sensor networks. There has been significant research in this area relating to node assignment, to include the work of Heo *et al*. [16] and Howard *et al*. [17] for network deployment.

Our research can be thought of as the converse to the assignment problem [20], where the final pose of the formation is known *a priori*, and the goal is to find an optimal assignment of nodes to objective positions. In contrast, we determine the optimal pose corresponding to the objective formation shape where assignments remain fixed across shape transitions.

III. Background and Problem Formulation

In its general form, a constrained optimization problem can be written as

$$\min_{x\in\Phi} f(x)$$
$$\Phi = \{x : h_i(x) \leq 0, \forall\, i \in \mathcal{I};\ g_i(x) = 0, \forall\, i \in \mathcal{E}\} \tag{1}$$

where $\mathcal{I}$ and $\mathcal{E}$, respectively, denote finite index sets corresponding to inequality and equality constraints, $x \in \mathbb{R}^n$ represents the decision variables, $f : \mathbb{R}^n \to \mathbb{R}$ is the objective function corresponding to the quantity(ies) we wish to optimize, $h_i : \mathbb{R}^n \to \mathbb{R}\ \forall\, i \in \mathcal{I}$ denotes inequality constraint functions, and $g_i : \mathbb{R}^n \to \mathbb{R}\ \forall\, i \in \mathcal{E}$ is the equality constraint functions. Both the inequality and equality constraints serve to limit the set of feasible values for x. In the context of motion planning, x would typically correspond to the concatenated position variables of the robot team. The inequality constraints h_i might be used to define vehicle kinematic constraints or workspace boundaries, while the equality constraints g_i might be used to specify the desired position for each robot with respect to a world coordinate frame $\mathcal{W}$ or relative to another robot.

For general constrained optimization problems, real-time solutions can typically be computed for only a small number of nodes—and often without guarantees of optimality. This makes the approach unattractive for large-scale formations. As such, we instead focus on the special class of problems where (1) is *convex*—i.e., the equations f, h_i are convex and g_i are affine [5]. We then apply convex optimization techniques to a range of motion planning tasks for fully actuated mobile robots, i.e., where

$$\dot{x} = u \quad x \in \mathcal{C} \quad u \in \mathcal{U} \tag{2}$$

and where $\mathcal{C}$ is assumed convex, and $\mathcal{U} \subseteq \mathbb{R}^2$ can be defined through a finite number of convex constraints. A fundamental property of convex problems is that local minima are *global* minima. As a consequence, solutions are globally optimal and can be obtained using algorithms with super-linear convergence properties. While the convexity assumptions are not insignificant, we will show that they still support a relatively rich framework for coordinating fully actuated robots. Extensions to nonconvex polygonal workspaces are also discussed in Section VIII.

To efficiently coordinate the robot team, we require a concise mathematical representation for the formation. For example, abstraction-based control approaches use low-dimensional representations such as bounding boxes or first/second-order statistics of the robot positions [3].

Instead, we employ *shape* for our formation representation. Shape has different meanings in different contexts. We use the definition from shape analysis [14].

Definition 3.1: The shape of a formation is the geometrical information that remains when location, scale, and rotational effects are removed.

Consider a formation of $m \geq 2$ robots in a Euclidean space $\mathbb{R}^k$, $k \in \{2, 3\}$. Let $s_i \in \mathbb{R}^k$ denote the position of the ith robot relative to some local frame $\mathcal{F}$. Without loss of generality, let s_1 correspond to the origin $O_{\mathcal{F}}$. We denote the formation by the $m \times k$ matrix

$$S = (s_1, \ldots, s_m)^T \tag{3}$$

which is the concatenated coordinates of our m robots in $\mathcal{F}$. We can then define the shape of S as the equivalence class of the full set of similarity transformations of the formation

$$[S] = \{\alpha SR + 1_m d^T : \alpha \in \mathbb{R}_+, R \in SO(k), d \in \mathbb{R}^k\} \tag{4}$$

where $\alpha \in \mathbb{R}_+$ is the scale, $R \in SO(k)$ is a rotation matrix, 1_m is the m-dimensional vector of 1's, and $d \in \mathbb{R}^k$ is the translation vector. Adopting standard convention, we let $Y \sim S$ denote an equivalence relation between Y and S (i.e., $Y \sim S \Leftrightarrow Y \in [S]$).

Shape provides a natural, higher level representation for describing formation pose. As such, we repose the motion planning problem to one of changing to (or maintaining) a given shape subject to workspace, velocity constraints, etc. We show that optimal shape changes—which minimize the distance the nodes must travel—can be achieved through second-order cone programming (SOCP) techniques.

Let the $m \times k$ matrix $P = (p_1, \ldots, p_m)^T$ denote the concatenated coordinates of the current formation pose in some world frame $\mathcal{W}$. Our objective is to obtain a new formation pose $Q = (q_1, \ldots, q_m)^T$ in $\mathcal{W}$ where Q has the same shape as S under the equivalence relation defined in (4), and where either the maximum distance between the respective positions in P and Q are minimized, or where the sum of the distances is minimized. We can formulate this as the following optimization problem.

Problem 3.2: Given an initial formation pose $P \subset \mathcal{W}$ and a formation shape icon $S \subset \mathcal{F}$, $P \not\sim S$, obtain a new formation pose $Q \subset \mathcal{W}$, $Q \sim S$ and where

1) $\max_{i=1,\ldots,m} \|q_i - p_i\|_2$ is minimized or;
2) $\sum_{i=1}^m \|q_i - p_i\|_2$ is minimized.

IV. Optimal Shape Changes via SOCP

Consider the case of fully actuated robots on the plane. We can then represent the shape of our icon S as

$$[S] = \{\alpha SR + 1_m d^T : \alpha \in \mathbb{R}_+, R \in SO(2), d \in \mathbb{R}^2\}. \tag{5}$$

Let $s_i = (s_i^x, s_i^y)$ and $q_i = (q_i^x, q_i^y)$ denote Cartesian coordinates in $\mathcal{F}$ and $\mathcal{W}$, respectively. Choosing $d \triangleq q_1$, (5) then represents a set of nonlinear equality constraints of the form

$$\left.\begin{aligned} q_i^x - q_1^x &= \alpha\left(s_i^x \cos\theta - s_i^y \sin\theta\right) \\ q_i^y - q_1^y &= \alpha\left(s_i^x \sin\theta + s_i^y \cos\theta\right) \end{aligned}\right\}, \qquad i = 2, \ldots, m \tag{6}$$

where θ corresponds to the orientation. Without loss of generality, we can define the formation orientation and scale, respectively, as

$$\theta = \arctan\frac{q_2^y - q_1^y}{q_2^x - q_1^x}, \qquad \alpha = \frac{\|q_2 - q_1\|_2}{\|s_2\|_2} \tag{7}$$

where $s_1 \triangleq O_{\mathcal{F}}$. Given these assignments, with a little algebra, we can rewrite the constraints in (6) as

$$\left.\begin{aligned} \|s_2\|_2\left(q_i^x - q_1^x\right) &= \left(s_i^x, -s_i^y\right)^T (q_2 - q_1) \\ \|s_2\|_2\left(q_i^y - q_1^y\right) &= \left(s_i^y, s_i^x\right)^T (q_2 - q_1) \end{aligned}\right\}, \qquad i = 3, \ldots, m. \tag{8}$$

These $2(m-2)$ constraints are now convex (in fact, linear) functions of our state vector $q = (q_1, \ldots, q_m)^T$. They are also *necessary and sufficient* for describing the formation shape [19]. Writing these constraints in matrix form $Aq = 0$, we see a further advantage is that they implicitly define a low-dimensional representation for the formation, as the dimension of the nullspace $\dim(\mathcal{N}(A)) = 4$. The four free variables correspond to the translation, rotation, and scale of the shape as defined in (5).

The problem of finding the formation pose Q can now be posed as either of the following constrained optimization problems

$$\begin{array}{ll} \min\limits_{q} & \max\limits_{i=1,\ldots,m} \|q_i - p_i\|_2 \\ \text{s.t.} & Aq = 0 \end{array} \qquad \begin{array}{ll} \min\limits_{q} & \sum\limits_{i=1}^{m} \|q_i - p_i\|_2 \\ \text{s.t.} & Aq = 0 \end{array} \tag{9}$$

where the former corresponds to our *minimax* distance metric defined in Problem 3.2.1 and the latter our *total distance* metric.

While both the constraints and objective functions of these problems are convex, the form of the latter does not lend itself to traditional optimization techniques. To remedy this, we augment the state vector q with an auxiliary variable t_1 for our minimax metric, and with m auxiliary variables $t = (t_1, \ldots, t_m)^T$ for our total distance metric. The problems in (9) can thus be restated

$$\begin{array}{lll} \min\limits_{q,t_1} & t_1 & \\ \text{s.t.} & y_i \leq t_1, \quad i = 1, \ldots, m & \\ & Aq = 0 & \end{array} \qquad \begin{array}{lll} \min\limits_{q,t} & 1_m^T t & \\ \text{s.t.} & y_i \leq t_i, & i = 1, \ldots, m \\ & Aq = 0 & \end{array} \tag{10}$$

where $y_i \triangleq \|q_i - p_i\|_2$.

Both forms are equivalent. However, the objectives in (10) are now twice differentiable. We have also introduced m convex second-order conic constraints. These problems are now second-order cone programs, and they can be solved efficiently using modern interior point algorithms [22].

A. Regulating Shape Parameters

Through the use of additional linear and second-order cone constraints, we can regulate the rotation, translation, and scale of the formation shape. Constraining the minimum and maximum orientation $(\theta_{\min}, \theta_{\max})$ can be accomplished through a pair of linear constraints

$$\begin{aligned} (q_2 - q_1)^T(-\sin\theta_{\max}, \cos\theta_{\max}) &\leq 0 \\ (q_2 - q_1)^T(\sin\theta_{\min}, \cos\theta_{\min}) &\leq 0. \end{aligned} \tag{11}$$

Constraining the translation and the maximum scale of the formation can be respectively done using second-order cone constraints

$$\|q_1 - p_1\|_2 \leq t_{\max}, \qquad \|q_2 - q_1\|_2 \leq \alpha_{\max}. \tag{12}$$

Note, however, that constraints of the form

$$\|q_2 - q_1\|_2 \geq \alpha_{\min}, \qquad \|q_2 - q_1\|_2 = \alpha \tag{13}$$

are *not* convex. If regulating the minimum scale is required, we have developed an efficient approximation method based upon our results for fixed orientations in $\mathbb{R}^2$ and $\mathbb{R}^3$. The interested reader is referred to [27] for further details.

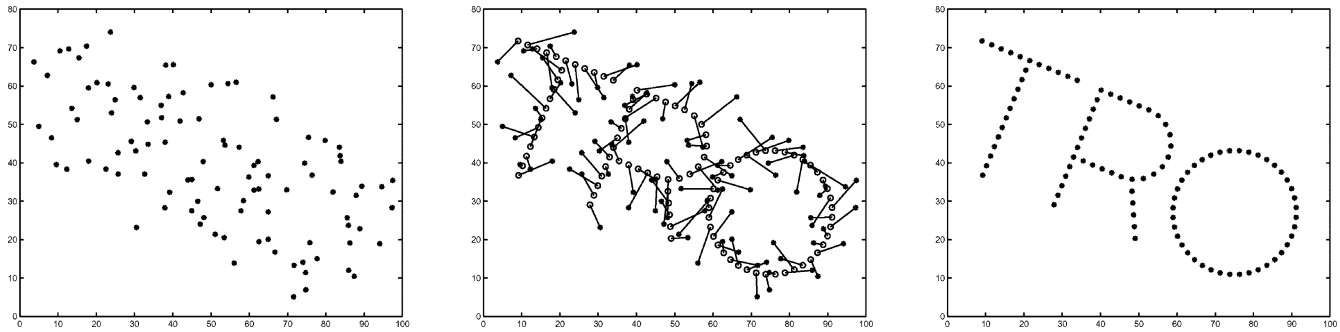

Fig. 1. Initial formation pose for a set of 100 nodes in $\mathbb{R}^2$ (left). The final formation trajectory/pose that achieves the desired shape while minimizing the total distance that the team must travel (center, right). The optimal values were 107.612 for scale, -22.403° for orientation, and $(9.059, 71.72)^T$ for translation.

B. Simulation Results

Fig. 1 shows a simulation trial demonstrating the process. In this example, 100 nodes were tasked with transitioning to a new shape while minimizing the total distance traveled. While deliberately contrived, this example demonstrates the efficacy of our approach. The formation is able to optimally transit from an arbitrary shape to a very specific shape. This would typically be the case when a formation of robots was initially deployed. In this example, none of the shape parameters (i.e., translation, rotation, or scale) were regulated.

V. On Complexity

To be suitable for use in large-scale formations, the shape problem needs to feature low computational complexity as well as be solvable in real time. In this section, we show that it can be solved in only $O(m^{1.5})$ basic operations. To this end, we employ a simple logarithmic barrier approach [5]. For the sake of brevity, the results presented here are specific to the *minimax* distance problem. However, we have obtained similar results for the *total distance* problem variation as well [11]. This includes both the regulated and unregulated shape problem formulations.

A. Reformulating the Shape Problem

The original *minimax* shape planning problem can be restated in a relaxed form suitable for solving via the barrier approach. Conversion requires augmenting the objective function given in (10) with log-barrier terms corresponding to the problem's conic constraints as follows

$$\begin{array}{ll} \min\limits_{q,t_1} & \tau_k t_1 - \sum\limits_{i=1}^{m} \log\left(t_1^2 - (q_i - p_i)^T (q_i - p_i)\right) \\ \text{s.t.} & Aq = 0 \end{array} \tag{14}$$

where τ_k is the inverse log-barrier scaler for the kth iteration. Essentially, solving our SOCPs reduces to solving a sequence of convex optimization problems of this form, where after each iteration τ_{k+1} is chosen such that $\tau_{k+1} = \mu^k \tau_k$ with $\mu \in \mathbb{R}, \mu > 1$ being an algorithmic constant.

B. Banding the Newton KKT System

During each iteration of the log-barrier approach, we aim to minimize the second-order Taylor approximation of our objective as a function of the Newton step δx subject to $A\,\delta x = 0$. As a result, obtaining δx is equivalent to analytically solving the Karush–Kuhn–Tucker (KKT) conditions associated with this equality-constrained subproblem [5]. In other words, we must solve the following linear system of equations [5]:

$$\begin{pmatrix} H & A^T \\ A & 0 \end{pmatrix} \begin{pmatrix} \delta x \\ w \end{pmatrix} = \begin{pmatrix} -g \\ 0 \end{pmatrix} \tag{15}$$

where H and g, respectively, denote the evaluated Hessian and gradient of the objective function given in (14) at x, w is the corresponding dual variable for δx, and A is as previously defined. Solving (15) is the bottleneck of the algorithm. However, we will show that it can be solved in linear time by reposing (14).

Noting that the coefficient matrix of (15) is symmetric indefinite, we employ Gaussian elimination with nonsymmetric partial pivoting. The performance of this technique suffers significantly when the linear system in question features dense rows and/or columns due to fill-in [26]. In particular, the algorithm would yield a worst case performance of $O(m^3)$ when solving (15) for the problem formulation given in (14). Such a workload is highly impractical when considering large-scale configurations that feature 1000's of decision variables. To address this issue, we instead employ an auxiliary formulation of (14) that facilitates transforming the Newton KKT system into a monobanded form

$$\begin{array}{ll} \min\limits_{q,t} & \frac{\tau_k}{m} \sum\limits_{i=1}^{m} t_i - \sum\limits_{i=1}^{m} \log\left(t_i^2 - (q_i - p_i)^T (q_i - p_i)\right) \\ \text{s. t.} & \|s_2\|_2 \left(q_l^x - d_j^x\right) = \left(s_l^x, -s_l^y\right)^T (d_{j+1} - d_j) \\ & \|s_2\|_2 \left(q_l^y - d_j^y\right) = \left(s_l^y, s_l^x\right)^T (d_{j+1} - d_j) \\ & t_{i+1} = t_i, \qquad i = 1, \ldots, m-1 \\ & d_{2i+1} = d_{2i-1}, \qquad i = 1, \ldots, m-3 \\ & d_{2(i+1)} = d_{2i}, \qquad i = 1, \ldots, m-3 \\ & d_i = q_i, i \in \{1, 2\} \end{array} \tag{16}$$

for $l = 3, \ldots, m$ and where $j = 2(i-3) + 1$.

Notice that the objective has changed; however, we see that both forms are equivalent since

$$\frac{\tau_k}{m} \sum_{i=1}^{m} t_i = \frac{\tau_k}{m} \sum_{i=1}^{m} t_1 = \left(\frac{\tau_k}{m}\right) m t_1 = \tau_k t_1 \tag{17}$$

where the first equality holds due to the constraints placed on t_i.

1) Banding the Linear System: Given this augmented formulation, our claim is that the system can be made monobanded. To show this, we begin by defining the initial solution vector ordering for (15) as it corresponds to problem (16) as follows:

$$\left(\delta\eta_1^T, \delta\eta_2^T, \delta\kappa_1^T, \ldots, \delta\kappa_{(m-2)}^T, \mu^T\right)^T$$

$$\delta\eta_i = \begin{pmatrix} \delta q_i \\ \delta t_i \end{pmatrix}, \quad \delta\kappa_i = \begin{pmatrix} \delta d_{2(i-1)+1} \\ \delta d_{2(i-1)+2} \\ \delta\eta_{(i+2)} \end{pmatrix}, \quad \mu = \begin{pmatrix} w_1 \\ \vdots \\ w_{7m-13} \end{pmatrix} \tag{18}$$

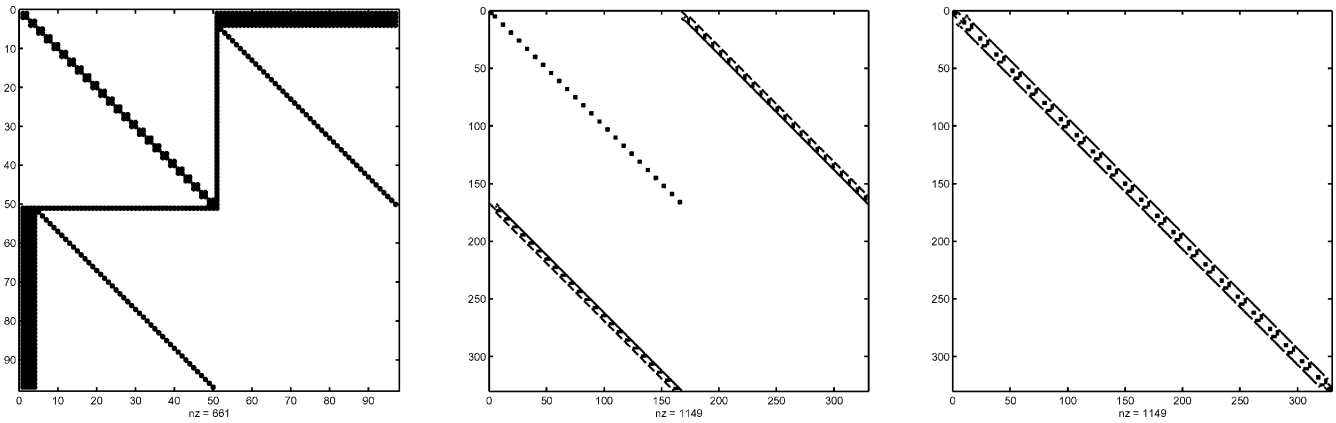

Fig. 2. Nominal Newton KKT system sparsity structure for the *minimax* motion planning problem in $SE(2)$ (left). Augmented Newton KKT system sparsity structure (center). The banded system with lower and upper bandwidths of 8 (right). This system is now solvable in $O(m)$ time.

where the δ variables correspond to the primal Newton step components associated with each of the system variables, and w_j denotes the dual variable associated with the $j\text{th}$ constraint.

In order to yield the monobanded form, we begin by stating the constraint/row permutation for A that yields the tribanded system appearing in Fig. 2 (center). We assume that A is already arbitrarily constructed with random row and column permutations. For the sake of clarity, we group constraints by associating them with the respective nodes that introduce them into the system. In doing so, we employ a slight abuse of notation by allowing q_i to also denote the $i\text{th}$ robot in the configuration. That stated, we now define the constraints associated with q_1 and q_2 as

$$\begin{aligned} \varrho_1 &\triangleq q_1^x = d_1^x & \qquad \varrho_4 &\triangleq q_2^x = d_2^x \\ \varrho_2 &\triangleq q_1^y = d_1^y & \qquad \varrho_5 &\triangleq q_2^y = d_2^y. \\ \varrho_3 &\triangleq t_1 = t_2 \end{aligned} \tag{19}$$

Similarly, for $3 \leq i \leq (m-1)$, we define the constraints associated with q_i as

$$\begin{aligned} \varphi_{i_1} &\triangleq \|s_2\|_2 \left(q_i^x - d_j^x\right) = \left(s_i^x, -s_i^y\right)^T \left(d_{j+1} - d_j\right) \\ \varphi_{i_2} &\triangleq \|s_2\|_2 \left(q_i^y - d_j^y\right) = \left(s_i^y, s_i^x\right)^T \left(d_{j+1} - d_j\right) \\ \varphi_{i_3} &\triangleq t_i = t_{i-1} \\ \varphi_{i_4} &\triangleq d_{j+2}^x = d_j^x \\ \varphi_{i_5} &\triangleq d_{j+2}^y = d_j^y \\ \varphi_{i_6} &\triangleq d_{j+3}^x = d_{j+1}^x \\ \varphi_{i_7} &\triangleq d_{j+3}^y = d_{j+1}^y \end{aligned} \tag{20}$$

where j is as defined previously.

With q_m, we associate the remaining three constraints

$$\begin{aligned} \varphi_{m_1} &\triangleq \|s_2\|_2 \left(q_m^x - d_j^x\right) = \left(s_m^x, -s_m^y\right)^T \left(d_{j+1} - d_j\right) \\ \varphi_{m_2} &\triangleq \|s_2\|_2 \left(q_m^y - d_j^y\right) = \left(s_m^y, s_m^x\right)^T \left(d_{j+1} - d_j\right) \\ \varphi_{m_3} &\triangleq t_m = t_{m-1} \end{aligned} \tag{21}$$

where j is as previously stated with $i = m$.

Again employing a slight abuse of notation, we let each φ_{i_j} denote the initial row index of its associated constraint. As such, we provide the following row permutation for A. This ordering yields the tribanded form appearing in Fig. 2 (center)

$$\left(\vartheta^T, \varkappa_1^T, \ldots, \varkappa_{(m-1)}^T, \varsigma^T\right)^T$$

$$\vartheta = \begin{pmatrix} \varrho_1 \\ \varrho_2 \\ \vdots \\ \varrho_5 \end{pmatrix}, \quad \varkappa_i = \begin{pmatrix} \varphi_{(i+2)_1} \\ \varphi_{(i+2)_2} \\ \vdots \\ \varphi_{(i+2)_7} \end{pmatrix}, \qquad \varsigma = \begin{pmatrix} \varphi_{m_1} \\ \varphi_{m_2} \\ \varphi_{m_3} \end{pmatrix} \tag{22}$$

Given this definition of A as well as (18), the monobanded form of (15) can be constructed. Symmetrically applying the permutation that yields the following solution vector ordering

$$\left(\lambda^T, \xi_1^T, \ldots, \xi_{(m-3)}^T, \chi^T\right)^T \tag{23}$$

$$\lambda = \begin{pmatrix} \delta\eta_1 \\ w_1 \\ \vdots \\ w_5 \\ \delta\eta_2 \end{pmatrix}, \quad \xi_i = \begin{pmatrix} \delta d_{2(i-1)+1} \\ \delta d_{2(i-1)+2} \\ w_{6+7(i-1)} \\ \vdots \\ w_{12+7(i-1)} \\ \delta\eta_{(i+2)} \end{pmatrix}, \qquad \chi = \begin{pmatrix} \delta d_{2m-5} \\ \delta d_{2m-4} \\ w_{7m-15} \\ w_{7m-14} \\ w_{7m-13} \\ \delta\eta_m \end{pmatrix}$$

produces a monobanded coefficient structure having a total bandwidth of 17.

Fig. 2 illustrates this process of transforming the Newton KKT system. The "augmented" system derived from the permutations given in (18) and (22) is shown in Fig. 2 (center). Taking the coefficient structure of (15) in this form and symmetrically permuting its rows and columns according to (23) yields the monobanded system appearing in Fig. 2 (right). It can now be solved in $O(m)$ using a band-diagonal lower–upper (LU)-based solver [25].

C. Complexity in Practice

Modern interior-point methods (IPMs) require $\sqrt{m}$ iterations to converge [22]. However, it is well known that this computational bound is extremely conservative, and that iteration complexity in practice is $O(1)$ [5]. Consequently, solving the shape problems requires only $O(m)$ basic operations in practice.

Simulation Results: A total of 20 000 instances of the unregulated total distance problem were solved using the Mosek industrial package [24]. Values of m were considered between 10 and 2000 using a step size of 10. For each configuration size, a total of 100 random problem instances were solved. All problems were solved on standard desktop

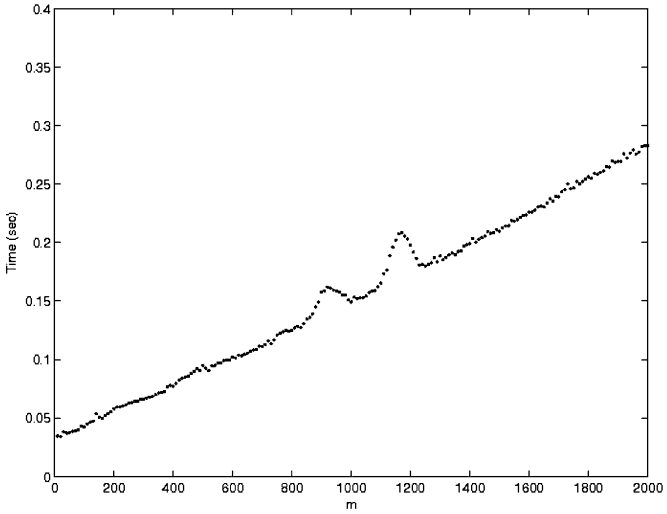

Fig. 3. Mean CPU time required to solve the unregulated total distance metric shape problem using the Mosek industrial solver. Each point corresponds to the mean for a sample of 100 randomly generated shape SOCPs. The trend is strongly linear with $r^2 = 0.9905$.

PC having a 3.0 GHz Pentium 4 processor. From Fig. 3, we see the time complexity scales as $O(m)$ with $r^2 = 0.9905$, where r is the correlation coefficient. *Furthermore, the data indicate that for a team of up to 2000 robots, the problem can be solved in less than 300 ms!*

VI. Integrating Motion Constraints

This framework relies upon the convexity of the underlying problem to efficiently solve coordination problems for large formations. As a consequence, motion constraints can also be accommodated so long as they can be expressed similarly. For example, to this point, we have generated objective node positions without consideration for vehicle constraints. However, we could readily accommodate velocity constraints as second-order cone constraints of the form

$$\|q_i - p_i\|_2 \leq v_i^{\max} \delta t \tag{24}$$

where δt denotes the time step, and $v_i^{\max}$ denotes the velocity limits of the ith robot. This would allow less mobile or even fixed (anchor) nodes to be accommodated. Others might be expressed as linear constraints. As an example, a formation wanting to maintain positive velocity in the y-direction could ensure this by specifying a minimum forward distance traveled $d_{\min}$ for each node as

$$q_i^y - p_i^y \geq v_i^{\min} \delta t, \qquad i \in \{1, \ldots, m\}. \tag{25}$$

In summary, if the constraints can be expressed in terms of some combination of *feasible* linear, second-order cone, or semidefinite constraints, they can be directly integrated into our framework. Furthermore, as with the environmental constraints discussed in Section VII, the motion constraints introduced by the ith node are only a function of its own initial and final positions. As a result, the monobanded structure and complexity results derived in Section V will again be preserved.

Simulation Results: A sample simulation showing the same formation shape change with (triangles) and without (circles) motion constraints is presented in Fig. 4. In both the cases, the objective was for the teams to transit from an initial in-line path configuration to a triangular shaped formation. Optimization was over our minimax metric. In the former, the minimum forward distance traveled for each node was constrained as $q_i^y - p_i^y \geq 0,\ i \in \{1, \ldots, m\}$. Scale and orientation were

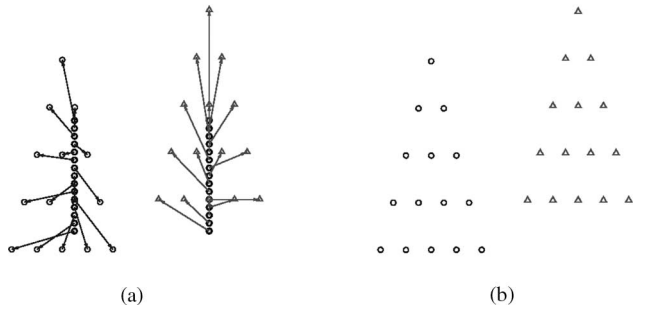

Fig. 4. Shape transitions for two teams of 15 robots, each respectively aligned along an in-line path. (a) In this case, the teams were charged with obtaining a triangular formation while minimizing the minimax distance metric. With no motion constraints (left). With $q_i^y - p_i^y \geq 0, i = 1, \ldots, m$ (right). (b) Final configurations obtained by the respective teams. Including the motion constraints increased the minimax distance for the formation by 87% in this case.

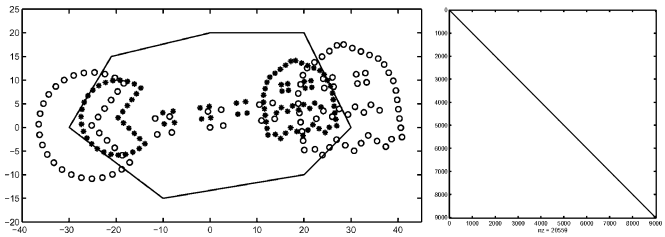

Fig. 5. Two problem instances with (stars) and without (circles) boundary constraints (left). In this example, the workspace limits constrained the scale of the optimal solution from $\alpha = 85$ to $\alpha = 59.85$. The monobanded form of the problem instance with workspace constraints (right).

fixed in both cases. In this case, the additional constraints increased the minimax distance for shape formation by 87%.

VII. Integrating Workspace Constraints

A straightforward extension to regulate the formation shape would be to ensure that the final configuration resides within the bounds of the operational environment. If we assume that the workspace $\mathcal{C}$ can be modeled via k linear inequalities yielding a convex space, e.g.,

$$\mathcal{C} = \{x \in \mathbb{R}^2 \colon A_c x \leq b_c\} \tag{26}$$

this will introduce km additional constraints where m again denotes the number of agents in the configuration. However, the core linear system will remain monobanded, as the k constraints introduced for the ith team member's position are only a function of the node's position in the final formation (i.e., q_i). Moreover, the coefficients of these constraints can be chained locally by introducing $2k$ auxiliary variables for each robot [12]. As a consequence, the linear system is solvable in $O(km)$ time, and the corresponding SOCP can be solved in $O(km)$ time in practice—or linear time in the size of the formation and the environment.

Simulation Results: In this example, we considered a variation of the shape problem where the objective function was modified to maximize the scale of the formation subject to workspace boundary constraints. Such a result might prove useful for tasks such as maximizing sensor network coverage while satisfying a desired shape geometry. In this example, the orientation of the shape was fixed. Fig. 5 illustrates the results obtained for a team of 101 nodes in $SE(2)$. Both constrained and unconstrained problem solutions are presented to illustrate the influence of the convex workspace model. The nonzero dot plot of the

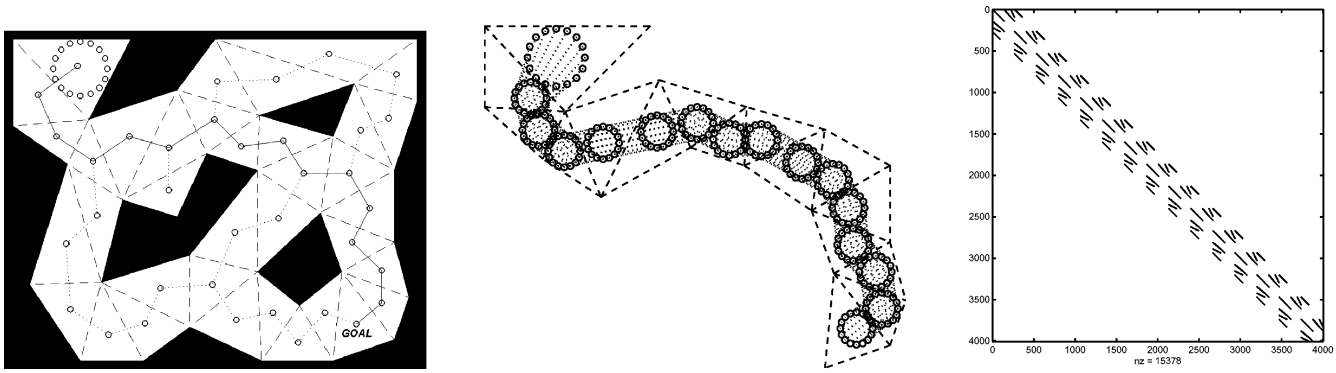

Fig. 6. $\mathcal{C}_{\text{path}}$ as specified by the higher level planner (left). The corresponding motion sequence obtained from solving the associated SOCP (center). The formation is guaranteed to follow $\mathcal{C}_{\text{path}}$ while minimizing the total distance traveled, avoiding obstacles, and maintaining the desired formation shape. In this example, the orientation and minimum scale for the formation were constrained. The linear system remains monobanded (right).

Newton KKT system is also shown to highlight that the monobanded structure of the linear system remains intact.

VIII. Motion Planning in Polygonal Environments

Extending the results of Section VII, we now consider motion planning in a polygonal environment with obstacles. Obstacles highlight a significant limitation of convexification approaches. Recall the underlying assumption of (26) was that the workspace could be defined through a finite number of convex constraints. When we introduce obstacles into the workspace, we create voids in the feasible set. The result is a loss of convexity, and the corresponding optimization problem becomes significantly more difficult to solve. While convex relaxations present one potential remedy [9], we instead take inspiration from [2] and employ a hierarchical discrete-continuous optimization approach.

We assume the configuration space for the robot team $\mathcal{C}$ is a polygonal environment with obstacle subspace $\mathcal{O}$ and free space $\mathcal{C}_{\text{free}}$ such that $\mathcal{C}_{\text{free}} = \mathcal{C} - \mathcal{O}$. Using exact cell decomposition methods (e.g., triangulation, trapezoidal decomposition, etc.), $\mathcal{C}_{\text{free}}$ can be tessellated into convex polygonal cells $C_1, \ldots, C_z$, where $\mathcal{C}_{\text{free}} = \cup_{i=1}^{z} C_i$ [6]. The resulting partition induces an undirected graph $G = (V, E)$, where vertex $v_i \in V$ corresponds to cell C_i, and edge $e_{ij} \in E$ implies that there exists a common edge between C_i and C_j. Paths between cells can then be efficiently computed using traditional graph optimization algorithms [13]. The motion planning problem can then be reposed as transitioning the formation from cell to cell along the specified path. In the sequel, we assume a triangulation partition of $\mathcal{C}_{\text{free}}$. We further assume that the union of adjacent cells $C_{ij} = C_i \cup C_j \ \forall \ (C_i, C_j) \in E$ is convex. While this may appear restrictive, it is straightforward to refine any pair of adjacent triangles to three such triangles where both of the resulting adjacent pairs meet this constraint.

Remark 8.1: Given two adjacent cells $(C_i, C_j) \in E$, where $C_{ij} = C_i \cup C_j$ is convex, if node $x_i \in C_i$ and $x_j \in C_j$, then by convexity $\lambda x_i + (1 - \lambda) x_j \in C_{ij},\ \lambda \in [0, 1]$. This implies that for a formation of m nodes with initial pose $X_i = (x_{i1}, \ldots, x_{im})^T \in \mathbb{R}^{2m}$ in triangle C_i, and final pose X_j in triangle C_j, the paths of each node will remain entirely in $C_{ij} \subseteq \mathcal{C}_{\text{free}}$. This guarantees against collisions with obstacles.

Let us assume that such a path $C_p = \{C_1, \ldots, C_k\} \subseteq \mathcal{C}_{\text{free}}$ has been specified by a higher level planner. Our motion planning problem can then be written as follows.

Problem 8.2: Given a path specification $C_p = \{C_1, \ldots, C_k\}$, a corresponding shape specification $S = \{S_1, \ldots, S_k\}$, and an initial formation pose X_0, find a motion sequence $X = \{X_1, \ldots, X_k\}$ for the formation such that

1) $X_i \sim S_i,\ i = 1, \ldots, k$;
2) $X_i \in C_i,\ i = 1, \ldots, k$;
3) the distance traveled by the formation is minimized in accordance with the criteria from Problem 3.2.

In solving Problem 8.2, we employ optimization techniques from model predictive control [18], [23]. In this context, however, the length of the horizon is not defined by time, but rather the length of the path over which the optimization problem is solved.

To constrain the pose of the formation during each step of the horizon, each triangle can be modeled as a set of three linear inequality constraints on the position of each node

$$c_{il}^T x_{ij} \leq 0, \quad i = 1, \ldots, k;\ j = 1, \ldots, m; l = 1, \ldots, 3. \tag{27}$$

In a slight abuse of notation, we also let $C_i = (c_{11}, \ldots, c_{m3})^T \in \mathbb{R}^{3m \times 2m}$ denote the set of linear constraints on the formation pose such that $X_i \in C_i$. We can now write the solution to Problem 8.2 for our total distance metric as

$$\begin{aligned} \min_{X} \quad & \sum_{i=1}^{k} \sum_{j=1}^{m} t_{ij}, \qquad i = 1, \ldots, k;\ j = 1, \ldots, m \\ \text{s.t.} \quad & \|x_{ij} - x_{i-1,j}\|_2 \leq t_{ij} \\ & A_i X_i = 0 \\ & C_i X_i \leq 0 \end{aligned} \tag{28}$$

where A_i are the constraints associated with shape $\mathcal{S}_i$ as defined in Section IV. This problem is also a SOCP.

More significantly perhaps, the corresponding Newton KKT matrix corresponds to the chaining of k instances of our single-step problem. As a result, the associated linear system will remain monobanded; however, in this case, the bandwidth will grow as either a function of m or k depending upon the selected permutation of the augmented KKT system. As such, we conclude the theoretical complexity is $O(k^{1.5} m^{3.5})$ or $O(k^{3.5} m^{1.5})$—once again depending upon the chosen ordering.

Simulation Results: A sample simulation trial for a formation of 16 robots is shown in Fig. 6. The path of the formation is specified by a higher level planner after a discrete optimization phase on the corresponding graph G (left). The formation then solves the continuous optimization problem specified in (28). The resulting path of the formation is shown in Fig. 6 (center). In this example, the optimization was over the entire path length $(k = 15)$, the shape was held constant, and the minimum scale of the formation was specified (as a premise for collision avoidance).

IX. Discussion

The thrust of this paper was to highlight the potential for employing convex optimization techniques to coordinate the motion of large-scale robot formations. Recent advances in the underlying algorithms allow large-scale motion planning problems to be solved online, and with a complexity that in practice scales linearly in the size of the formation and/or the environment. Key to our results was a formal definition of shape for describing the formation pose. This provides an implicitly low-dimensional representation that can be defined via linear equality constraints. Optimal shape changes can then be solved as SOCPs.

Worth noting is that our framework also lends itself to a distributed implementation that affords expected per node computational, message, and storage complexities of $O(1)$ [10]. It can be adapted for use with any IPM that preserves the separability of the objective with respect to each team member.

The convexity requirement has its limitations, such as when considering nonholonomic kinematic motion models. However, the optimal paths generated for the fully actuated robots can still be *followed* by differential drive/tracked vehicles, which see widespread use in mobile robotics. Although the results will no longer be optimal for such robots, they should still be quite good in practice. We should also point out that while the work presented in this paper focused on operations in the plane, we have similar results in $\mathbb{R}^3$ for fixed orientations [27]. Extending these results to operations in $SE(3)$ is currently a topic of ongoing research.

Other extensions to this research are also possible. One of our current interests is formation/network coverage and using robust estimation techniques to relax the shape constraints for improving system performance. We are also exploring ways to generalize our problem so as to provide optimal node assignments while yielding an optimal shape formation pose. Finally, the problem of finding optimal shape changes relates to the point pattern matching problem [28], and we are looking to apply our results to this as well as point-wise deformations in computer graphics.

Acknowledgment

The authors thank A. Jadbabaie for discussions on IPM complexity and R. Fierro on the coordination of robot formations.

References

[1] R. Bachmayer and N. E. Leonard, "Vehicle networks for gradient descent in a sampled environment," in *Proc. IEEE Conf. Dec. Control*, Las Vegas, NV, Dec. 2002, pp. 112–117.

[2] C. Belta, V. Isler, and G. Pappas, "Discrete abstractions for robot motion planning and control in polygonal environments," *IEEE Trans. Robotics*, vol. 21, no. 5, pp. 864–874, Oct. 2005.

[3] C. Belta and V. Kumar, "Abstraction and control for groups of robots," *IEEE Trans. Robot. Automat.*, vol. 20, no. 5, pp. 865–875, Oct. 2004.

[4] C. Belta and V. Kumar, "Optimal motion generation for groups of robots: A geometric approach," *ASME J. Mech. Des.*, vol. 126, pp. 63–70, 2004.

[5] S. Boyd and L. Vandenberghe, *Convex Optimization*. Cambridge, U.K.: Cambridge Univ. Press, 2004.

[6] H. Choset, K. Lynch, S. Hutchinson, G. Kantor, W. Burgard, L. Kavraki, and S. Thrun, *Principles of Robot Motion Planning*. Cambdrige, MA: MIT Press, 2005.

[7] J. Cortés, S. Martínez, T. Karatas, and F. Bullo, "Coverage control for mobile sensing networks," *IEEE Trans. Robot. Automat.*, vol. 20, no. 2, pp. 243–255, Apr. 2004.

[8] A. K. Das, R. Fierro, V. Kumar, J. P. Ostrowski, J. Spletzer, and C. J. Taylor, "A vision-based formation control framework," *IEEE Trans. Robot. Automat.*, vol. 18, no. 5, pp. 813–825, Oct. 2002.

[9] A. d' Aspremont and S. Boyd, *Relaxations and Randomized Methods for Nonconvex QCQPs*, Stanford Univ., Stanford, CA, 2003.

[10] J. Derenick, C. Mansley, and J. Spletzer, "Efficient motion planning strategies for large-scale sensor networks," in *Proc. 7th Int. Workshop Algorithmic Found. Robot. (WAFR 2006)*, New York, NY.

[11] J. Derenick and J. Spletzer, "TR LU-CSE-05-029: Optimal shape changes for robot teams," Lehigh Univ., Bethlehem, PA, Tech. Rep., 2005.

[12] J. Derenick and J. Spletzer, "Second-order cone programming (SOCP) techniques for coordinating large-scale robot teams in polygonal environments," *Advances Coop. Control Optim.*, to be published.

[13] E. Dijkstra, "A note on two problems in connexion with graphs," *Numer. Math.*, vol. 1, pp. 269–272, 1959.

[14] I. L. Dryden and K. V. Mardia, *Statistical Shape Analysis*. Hoboken, NJ: Wiley, 1998.

[15] J. T. Feddema, R. D. Robinett, and R. H. Byrne, "An optimization approach to distributed controls of multiple robot vehicles," presented at the Workshop Control Coop. Intell. Miniature Robots, IEEE/RSJ IROS, Las Vegas, NV, Oct. 31, 2003.

[16] N. Heo and P. K. Varshney, "Energy-efficient deployment of intelligent mobile sensor networks," *IEEE Trans. Syst., Man, Cybern. A, Syst., Humans*, vol. 35, no. 1, pp. 78–92, 2005.

[17] A. Howard, M. J. Mataric, and G. S. Sukhatme, "An incremental self-deployment algorithm for mobile sensor networks," *Auton. Robots*, vol. 13, no. 2, pp. 113–126, Sep. 2002.

[18] A. Jadbabaie, J. Yu, and J. Hauser, "Unconstrained receding-horizon control of nonlinear systems," *IEEE Trans. Autom. Control*, vol. 46, no. 5, pp. 776–783, May 2001.

[19] D. Kendall, D. Barden, T. Carne, and H. Le, *Shape and Shape Theory*. Hoboken, NJ: Wiley, 1999.

[20] H. W. Kuhn, "The Hungarian method for the assignment problem," *Naval Res. Logistics Quart.*, vol. 2, pp. 83–97, 1955.

[21] S. LaValle and S. Hutchinson, "Optimal motion planning for multiple robots having independent goals," *IEEE Trans. Robot. Automat.*, vol. 14, no. 6, pp. 912–925, Dec. 1998.

[22] M. Lobo, L. Vandenberghe, S. Boyd, and H. Lebret, "Applications of second-order cone programming," *Linear Algebra Appl., Special Issue Linear Algebra Control, Signals Image Process.*, vol. 284, pp. 193–228, 1998.

[23] D. Mayne, J. Rawings, C. Rao, and P. Scokaert, "Constrained model predictive control: Stability and optimality," *Automatics*, vol. 36, no. 6, pp. 789–814, Jun. 2000.

[24] MOSEK ApS, *The MOSEK Optimization Tools Version 3.2 (Revision 8) User's Manual and Reference* [Online]. Available: http://www.mosek.com/fileadmin/products/3/tools/doc/html/tools/tools.html

[25] W. H. Press, B. P. Flannery, S. A. Teukolsky, and W. T. Vetterling, *Numerical Recipes in C*. Cambridge, U.K.: Cambridge Univ. Press, 1993.

[26] Y. Saad, *Iterative Methods for Sparse Linear Systems*. Philadelphia, PA: SIAM, 2003.

[27] J. Spletzer and R. Fierro, "Optimal positioning strategies for shape changes in robot teams," in *Proc. IEEE Int. Conf. Robot. Automat.*, 2005, pp. 742–747.

[28] P. B. V. Wamelen, Z. Li, and S. S. Iyengar, "A fast algorithm for the point pattern matching problem," *Pattern Recog.*, vol. 37, no. 8, pp. 1699–1711, Aug. 2004.

[29] F. Zhang, M. Goldgeier, and P. S. Krishnaprasad, "Control of small formations using shape coordinates," in *Proc. IEEE Int. Conf. Robot. Automat.*, Taipei, Taiwan, R.O.C.S, Sep. 2003, vol. 2, pp. 2510–2515.